Vector-Based 3D Graphic Statics: a framework for the design of spatial structures based on the relation between form and forces

Pierluigi D'acunto , Jean-Philippe Jasienski , Patrick Ole Ohlbrock , Corentin Fivet , Joseph Schwartz , Denis Zastavni

PII: S0020-7683(19)30081-2
DOI: https://doi.org/10.1016/j.ijsolstr.2019.02.008
Reference: SAS 10277

To appear in: *International Journal of Solids and Structures*

Received date: 25 September 2018
Revised date: 23 January 2019

Please cite this article as: Pierluigi D'acunto , Jean-Philippe Jasienski , Patrick Ole Ohlbrock , Corentin Fivet , Joseph Schwartz , Denis Zastavni , Vector-Based 3D Graphic Statics: a framework for the design of spatial structures based on the relation between form and forces, *International Journal of Solids and Structures* (2019), doi: https://doi.org/10.1016/j.ijsolstr.2019.02.008

Vector-Based 3D Graphic Statics: a framework for the design of spatial structures based on the relation between form and forces

Pierluigi D'ACUNTO[a], Jean-Philippe JASIENSKI[b], Patrick Ole OHLBROCK[a], Corentin FIVET[c], Joseph SCHWARTZ[a], Denis ZASTAVNI[b]

[a] ETH Zurich, Institute of Technology in Architecture, Chair of Structural Design,
Stefano-Franscini-Platz 1, 8093 Zurich (CH)
dacunto@arch.ethz.ch

[b] UCLouvain, LOCI – Structures & Technologies

[c] EPF Lausanne, ENAC, Structural Xploration Lab

Abstract

This article develops a vector-based 3D graphic statics framework that uses synthetic and intuitive graphical means for the analysis and design of spatial structures such as networks of bar elements in static equilibrium. It is intended to support the collaborative work of structural engineers and architects from the conceptual phase of the design process. Several procedures for the construction of a vector-based 3D force diagram for any given 3D form diagram with an underlying planar or non-planar graph are identified and described. In the non-planar case, the proposed procedures rely on the preliminary topological planarization of the graph by cutting the crossing edges and reconnecting them to one or more newly inserted auxiliary vertices. The resulting planar graph can be then used as a base for the assembly of the 3D force diagram, without altering the static equilibrium of the structure. An implementation of the proposed framework to real design scenarios is presented through two case studies. These examples show how to take advantage of the bi-directional manipulation of the diagrams in the structural design process.

Keywords: structural design; static equilibrium; graphic statics; form diagram; force diagram; reciprocal diagrams; planar graph; planarization; parallel transformations; constraint-driven transformations.

1. Introduction

1.1. Traditional 2D graphic statics

Graphic statics is a set of geometric constructions that relate the form of a structure in static equilibrium with the forces acting on it. It is based on two reciprocal diagrams (Maxwell, 1864): a *form diagram* that represents the geometry of the structure together with its external forces; a *force diagram* that embeds a synthetic vector representation of the forces applied to

each node of the structure. Graphic statics was initially formulated in the second half of the 19th Century by Maxwell (1864), Rankine (1864), Culmann (1866), and Cremona (1872) among others. First applied as a mean to analyse 2D structures, structural designers soon recognised it as a unique method for finding new structural forms (Huerta, 2010). For instance, in 1929 Robert Maillart made use of it to define the shape of the Salginatobel Bridge in Switzerland as a negotiation between given boundary conditions and the minimisation of bending moments (Fivet and Zastavni, 2012).

1.2. Graphic statics in 3D

The extension of graphic statics to the third dimension opens up new opportunities for both the analysis and the design of spatial structures. Among the various strategies to handle graphic statics in 3D (Jasienski *et al.*, 2014), two have been predominantly studied in the last few years: the *polyhedron-based* and the *vector-based* approaches (Konstantatou *et al.*, 2018).

The polyhedron-based approach, initially introduced by Rankine (1864) and later developed by Maxwell (1867), considers a force diagram built as an assembly of *force polyhedral cells* (Figure 1b) with areas equivalent to force magnitudes. General procedures to construct and manipulate polyhedron-based form and force diagrams have been developed only recently (Akbarzadeh *et al.* 2015; Lee *et al.*, 2018; Konstantatou *et al.*, 2018).

The vector-based approach, whose general features have been highlighted by Maxwell (1864), considers a force diagram made out of *closed cycles of force vectors* – also defined as *force polygons* – whose lengths are equivalent to force magnitudes (Figure 1c). From a topological standpoint, vector-based form and force diagrams follow a *3D duality*, where form edges/vectors are mapped to force edges/vectors, form nodes to closed cycles of force vectors and closed cycles of form vectors to force nodes (Konstantatou *et al.*, 2018). In compliance with the convention of Cremona diagrams in 2D, corresponding edges in the two diagrams are parallel to each other (Jasienski *et al.*, 2016).

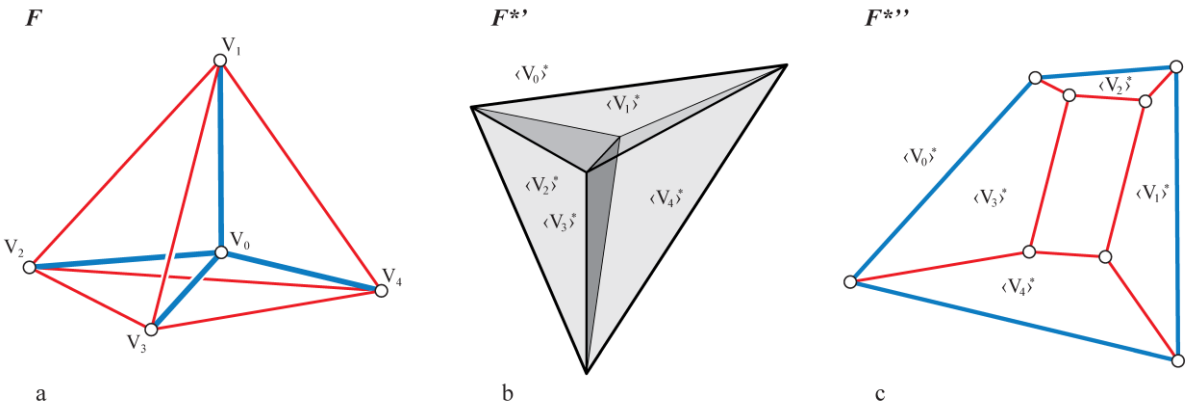

Figure 1: (a) 3D form diagram ***F*** of a self-stressed tetrahedron; (b) corresponding polyhedron-based 3D force diagram ***F*'**; (c) corresponding vector-based 3D force diagram ***F*''**.

Vector-based representations in 3D present certain benefits over their polyhedron-based counterparts. As pointed out by Maxwell (1864), it is always possible to construct force diagrams with vectors, as long as the structure is in static equilibrium. Besides, the use of vectors implies a higher accuracy in quantitative perceptual tasks (Mackinlay, 1986) and it is visually closer to traditional 2D graphic statics. Although vector-based 3D form and force diagrams generally lack reciprocity, the applicability of the vector-based approach to actual structural problems is guaranteed by the ability to transform both diagrams while preserving their topology, the parallelism of corresponding edges and the relationship between corresponding nodes and closed cycles of vectors.

1.3. Content and notation

This article introduces a consistent framework grounded on vector-based 3D graphic statics to support the analysis and design of any class of spatial networks of bar elements in static equilibrium, like pin-jointed frameworks and strut-and-tie models within a continuum of material.

Following the introduction in Section 1, Section 2 deals with the assembly of vector-based 3D force diagrams. After highlighting the conditions for the existence of reciprocal vector-based 3D diagrams, various procedures for the construction of 3D force diagrams are introduced and discussed following a graph theoretical approach; as explained, these procedures require the preliminary evaluation of the static equilibrium of the structure. Section 3 exemplifies two applications of vector-based 3D graphic statics to structural design: a suspended bridge and a stadium roof. A design workflow is described that takes advantage of the transformation of

3D form and force diagrams for the definition of the geometry and the control of the inner forces of the structures. The last section presents a synthesis of current research results.
In this article, the vector-based 3D form and force diagrams are referred to as ***F*** and ***F**** respectively. ***T*** is used to designate the underlying graph of ***F***. $\boldsymbol{T_P}$ refers to a planar embedding (i.e. plane graph) of ***T***; in case ***T*** is not planar, it is first transformed into a planar graph. $\boldsymbol{T_P^*}$ is the planar embedding of the dual graph of $\boldsymbol{T_P}$, which corresponds to the underlying graph of ***F****. The notations used for the individual elements of the graphs and diagrams are shown in Table 1. As a convention, in the figures red is used for tension, blue for compression and dark green for external forces.

Table 1 Notation used to describe vertices/nodes, edges and faces/closed cycles of vectors in ***T***, $\boldsymbol{T_P}$, ***F***, ***F****, and $\boldsymbol{T_P^*}$.

FORM	***T***, $\boldsymbol{T_P}$	***F***	***F****	$\boldsymbol{T_P^*}$	***FORCE***
vertex/node	v_i	V_i	$\langle V_i \rangle^*$	$\langle v_i \rangle^*$	face/closed cycle of force vectors
edge/form edge	e_{i-j}	E_{i-j}	E_{i-j}^*	e_{i-j}^*	force edge/edge
face/closed cycle of form vectors	$\langle v_i \rangle$	$\langle V_i \rangle$	V_i^*	v_i^*	vertex/node

2. Assembly of vector-based 3D force diagrams

The *closed cycles of force vectors* of a force diagram ***F**** represent the translational equilibrium of the nodes of the form diagram ***F***. Each pair of opposite forces acting within the same edge of ***F*** is represented in ***F**** as two opposite force vectors, which belong to two distinct closed cycles. When two such opposite force vectors overlap in ***F****, a *force edge* of similar position, angle, and length replaces them. If the resulting number of edges is equal in ***F*** and ***F****, the diagrams are *reciprocal* (Crapo, 1979). Otherwise, as it is usually the case in three-dimensional networks, a set of *non-overlapping force vectors* exists, and the diagrams are not reciprocal in the strict sense (Figure 2). Such circumstance is not a peculiarity of spatial structures as it also occurs in specific two-dimensional structures (Cremona, 1872). As explained in the next sections, this limitation is here dealt with by adding one or more new auxiliary cycles of force vectors to ***F****, hence generating pairs of *duplicate force edges*.

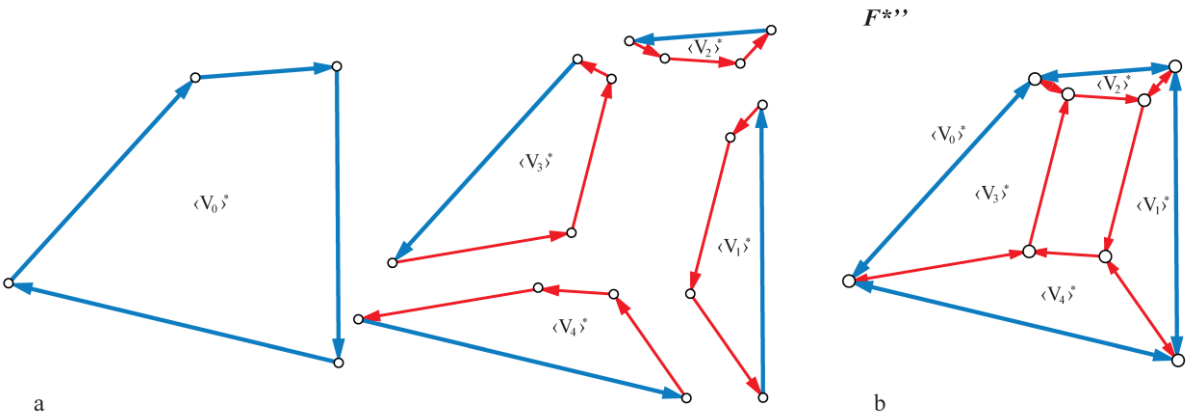

Figure 2: (a) individual closed cycles of force vectors representing the static equilibrium of each node in the self-stressed tetrahedron of Figure 1a; (b) assembly of the cycles shown in (a); note that two pairs of vectors are not overlapped.

2.1. Conditions for reciprocal vector-based 3D diagrams

Whitney (1933) demonstrated that a graph has a dual if and only if it does not contain a Kuratowski's subgraph – i.e. a subgraph that is a subdivision of K_5 or $K_{3,3}$ being the former the complete graph on five vertices and the latter the complete bipartite graph on six vertices (Harary, 1969). This condition results in the graph being *planar*. A graph is planar if it can be embedded in the plane or on the surface of a sphere, without edges crossing each other except at the vertices. As highlighted by Crapo (1979), any planar and three-connected graph – i.e. a graph that can be disconnected after the removal of a minimum of three vertices – is, at least topologically, the projection of a spherical polyhedron. Based on *Maxwell's theorem* (Crapo and Whiteley, 1993), the necessary and sufficient condition for a given truss to have a reciprocal on its dual graph is that its underlying graph is planar and that the structure supports a non-null self-stress state – i.e. a self-stress state that is non-zero on all edges of the structure.

Spatial structures in static equilibrium with underlying planar graphs are, for example, meshes composed of bars in space (Sauer, 1970; Wallner and Pottmann, 2008; and Tachi, 2012), some common tensegrity structures (Micheletti, 2008) or the dependent cube and octahedron (Crapo, 1979). Their vector-based reciprocal force diagrams, whose edges are parallel to the corresponding edges in the form diagram, have been denominated *Cremona Reciprocals* (Crapo 1979). However, as the underlying graph of 3D structures is generally non-planar, reciprocity between ***F*** and ***F**** is generally not achieved (Jasienski *et al.*, 2016). Several strategies to extend the concept of reciprocity to ***F*** and ***F**** with underlying non-planar graphs in both 2D and 3D cases are available in the literature. Among others, Bow (1873) added an

extra node at the intersection of bars in 2D trusses, Crapo and Whiteley (1993) addressed reciprocals as infinite frameworks, and Micheletti (2008) focused on point-symmetric reciprocal diagrams of some 3D self-stressed networks (Section 2.4.4). When reciprocal diagrams cannot be constructed, multiple alternative configurations of ***F**** can be generated for a given ***F***. Nevertheless, these different configurations still represent the same equilibrium state. A general procedure for the construction of 3D force diagrams in the non-planar case is introduced and described in this article (Section 2.4.1).

2.2. Evaluation of static equilibrium

Before constructing the force diagram ***F**** of a given form diagram ***F***, it is necessary to assess the magnitudes of the reaction forces at the supports, if any, and the magnitudes of the internal forces. The static and kinematic determinacy of a spatial network as a form diagram ***F*** is here evaluated with the *extended Maxwell rule* (Calladine, 1978):

$$s - m = E - 3V + k \tag{1}$$

where *s* is the number of independent states of self-stress, *m* of internal inextensible mechanisms, *E* of form edges, *V* of nodes and *k* of independent kinematic restraints at the supports (6 if the structure is not supported).

When the structural network is internally rigid and externally statically determinate, the equilibrium between applied loads and reactions is resolved before the evaluation of internal equilibrium. When the network is internally rigid and externally statically indeterminate, those support forces other than the ones necessary to attain the static determinacy are regarded as parameters. Given $\mathbf{q_i}$ applied loads, the $\mathbf{r_{Si}}$ reactions forces at the supports can be found using graphical procedures (D'Acunto *et al.*, 2016). This results in the generation of a *closed cycle of external force vectors* and the fulfilment of the following equilibrium conditions:

$$\mathbf{r} = \sum_i \mathbf{q_i} + \sum_i \mathbf{r_{Si}} = 0 \qquad \mathbf{m_O} = \sum_i \mathbf{p_i} \times \mathbf{q_i} + \sum_i \mathbf{p_i} \times \mathbf{r_{Si}} = 0 \tag{2}$$

where $\mathbf{r}$ and $\mathbf{m_O}$ are respectively the *resultant force* and the *resultant couple* of the system of forces regarding an arbitrarily chosen reference point O in space; $\mathbf{p_i}$ is the position vector of a point on the line of action of the force $\mathbf{q_i}$ (respectively $\mathbf{r_{Si}}$) in relation to O.

If the given structure is internally statically indeterminate, the inner self-stresses are treated as parameters when assessing internal equilibrium. Static equilibrium of internal forces can be solved node-by-node graphically (Jasienski *et al.*, 2016), leading to the creation of a *closed cycle of force vectors* for each node of the structure. That is, for each node V_i of ***F***,

considering the indexes j of all the nodes V_j connected to V_i and the related internal forces $\mathbf{f_{i-j}}$, the unknown force magnitudes μ_{i-j} are determined using the following expression:

$$\sum_j(\mathbf{f_{i-j}}) + \mathbf{q_i} + \mathbf{r_{Si}} = \sum_j(\mu_{i-j}\mathbf{d_{i-j}}) + \mathbf{q_i} + \mathbf{r_{Si}} = 0 \quad (3)$$

including the $\mathbf{q_i}$ and $\mathbf{r_{Si}}$ if present and where the unit vector $\mathbf{d_{i-j}}$ is obtained as:

$$\mathbf{d_{i-j}} = \frac{\mathbf{p_j}-\mathbf{p_i}}{||\mathbf{p_j}-\mathbf{p_i}||} \quad (4)$$

in which $\mathbf{p_i}$ is the position vector of V_i and $\mathbf{p_j}$ is the position vector of a node V_j connected to V_i. The equilibrium of a node can be solved using this procedure if the number of unknown μ_{j-i} is less or equal to three. When this graphical procedure cannot be applied, the more general algebraic approach that relies on the use of the *equilibrium matrix* **A** of the structure (Pellegrino and Calladine, 1986) can be employed.

2.3. Construction of 3D diagrams with underlying planar graphs

In the following, a geometric method is described to construct the force diagram ***F**** of a given form diagram ***F*** with underlying planar graph ***T***. This can be regarded as a direct extension to the third dimension of the customary graphic statics procedure given by Bow (1873) and Saviotti (1888) for solving 2D trusses with underlying planar graphs.

2.3.1. Self-stressed structures

When considering a self-stressed structure (Figure 3), the first step consists in converting the planar graph ***T*** into a plane graph $\boldsymbol{T_P}$, i.e. a drawing of ***T*** in the plane where edges are represented by non-crossing curves. Various algorithms of such planarization are found in the literature (Tamassia, 2013). In the second step, for each vertex v_i of $\boldsymbol{T_P}$ corresponding to the node V_i of ***F***, the indices of the incident edges e_{i-j} are listed in $\mathbf{l_i}$ following a *cyclic order* around v_i (e.g. counter-clockwise direction). In the third step, for each node V_i of ***F***, the free force vectors $\mathbf{f_{i-j}}$* equivalent in magnitude and direction to the inner forces $\mathbf{f_{i-j}}$ applied to V_i (Section 2.2) are arranged in a closed cycle of force vectors $<V_i>$*. The list $\mathbf{l_i}$ is used to define the sequence of the force vectors in $<V_i>$*. The cycles of force vectors $<V_i>$* are successively assembled into one single diagram ***F****, following the connectivity of the corresponding vertices in $\boldsymbol{T_P}$. That is, any two cycles of force vectors $<V_m>$* and $<V_n>$* are connected to each other if their corresponding nodes v_m and v_n in $\boldsymbol{T_P}$ share the same edge e_{m-n}. The connection between the cycles of force vectors is attained by overlapping the opposite

force vectors of $<V_m>^*$ and $<V_n>^*$, which relate to the common edge e_{m-n}, into one single edge E_{m-n}^* in ***F****.

F* built following this procedure is reciprocal to ***F***, i.e. *Cremona reciprocal* (Crapo, 1979). Hence, each node and cycle of edges in ***F*** has a corresponding closed cycle of edges and a node in ***F**** respectively. Moreover, each edge of ***F*** has one and only one corresponding edge in ***F****. The inverse is also true, and ***F**** itself can be regarded as a self-stressed structure. As such, the topologies of ***F*** and ***F**** are represented by $\boldsymbol{T_P}$ and its dual graph $\boldsymbol{T_P}^*$ respectively. The procedure here described is illustrated in Figure 3 using a dependent (self-stressed) structure, which is topologically a cube, as form diagram ***F*** and its reciprocal dependent structure, which is topologically an octahedron, as force diagram ***F**** (Crapo, 1979). The same is applied to a point-symmetric tensegrity (Figure 4) based on the Jessen's icosahedron (Jessen, 1967).

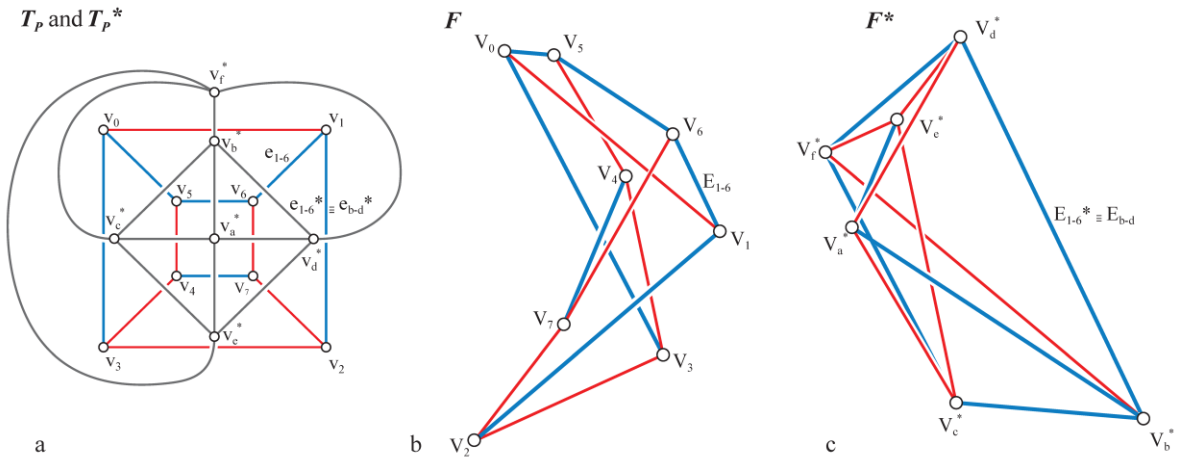

Figure 3: (a) Plane graph $\boldsymbol{T_P}$ (in colours) of a dependent cube and the dual $\boldsymbol{T_P}^*$ (in black) of its reciprocal dependent octahedron; (b) 3D form diagram ***F*** of a dependent cube: note that three coplanar edges are incident to each node; (c) reciprocal 3D force diagram ***F****: if regarded as a structure in its own right, ***F**** represents the form diagram of a dependent octahedron, while ***F*** is its reciprocal force diagram.

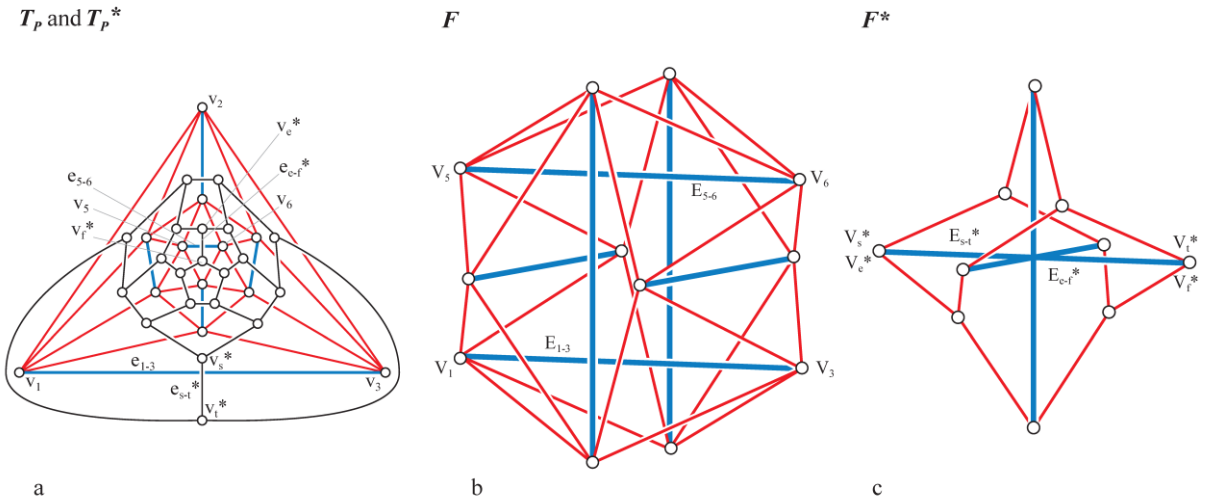

Figure 4: (a) Plane graph $\boldsymbol{T_P}$ of a Jessen's icosahedron and its dual $\boldsymbol{T_P}$*; (b) 3D form diagram $\boldsymbol{F}$ of the Jessen's icosahedron; (c) reciprocal 3D force diagram $\boldsymbol{F}$*: if regarded as the 3D form diagram of a structure with all duplicated elements, $\boldsymbol{F}$ is its reciprocal force diagram.

2.3.2. Externally loaded structures

If external forces are present in $\boldsymbol{F}$, these are denoted in $\boldsymbol{T}$ as edges e_{Ei}. Each e_{Ei} has one of its endpoints connected to the vertex of $\boldsymbol{T}$ that corresponds to the node of $\boldsymbol{F}$ where the external force is applied (Pirard, 1950). The other endpoint is connected to the *vertex of the external forces* v_E, an auxiliary element of $\boldsymbol{T}$ that does not have any corresponding node in $\boldsymbol{F}$ (Jasienski *et al.*, 2016). The vertex v_E can be regarded as the topological representation of a new structure in static equilibrium with forces opposite to the external forces applied to $\boldsymbol{F}$, and which would convert $\boldsymbol{F}$ into a self-stressed structure (Fivet, 2016). After embedding $\boldsymbol{T}$ in the plane to create $\boldsymbol{T_P}$, the methodology to construct $\boldsymbol{F}$* is equivalent to the second and third steps of the procedure described in Section 2.3.1. In this case, a cycle of external force vectors $<V_E>$* is also created, which relates to v_E and represents the equilibrium of the external forces (D'Acunto *et al.*, 2017). The topologies of $\boldsymbol{F}$ and $\boldsymbol{F}$* are represented respectively by $\boldsymbol{T_P}$, which includes the vertex of the external forces v_E, and its dual $\boldsymbol{T_P}$* (Figure 5).

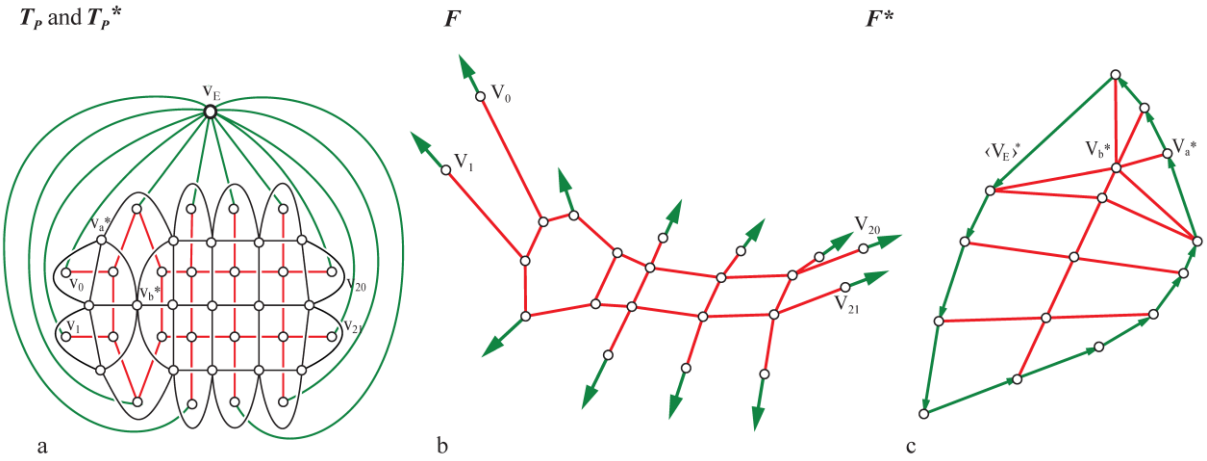

Figure 5: Externally loaded cable-net; (a) plane graph $\boldsymbol{T_P}$ and its dual $\boldsymbol{T_P}$*; (b) 3D form diagram $\boldsymbol{F}$; (c) 3D force diagram **F***.

2.3.3. Algebraic approach

The procedures previously described are comparable to the algebraic approaches defined by Van Mele *et al.* (2014), Alic and Akesson (2017), and Micheletti (2008), for 2D and 3D structures with underlying planar graphs. In fact, it is possible to generate an *oriented graph* $\boldsymbol{T_{PO}}$ from $\boldsymbol{T_P}$, by assigning an orientation to every edge of $\boldsymbol{T_P}$. The *incidence matrix* $\mathbf{C_0}$ of $\boldsymbol{T_{PO}}$ is then defined. Based on $\mathbf{C_0}$, the equilibrium matrix **A** is assembled, from which the magnitudes of the forces applied to the nodes of $\boldsymbol{F}$ are found (Micheletti, 2008). The *cycle space* of $\boldsymbol{T_{PO}}$ is defined as the orthogonal complement of the *row space* of $\mathbf{C_0}$, and each of the elements of one of its basis corresponds to a face of $\boldsymbol{T_{PO}}$. As explained by Micheletti (2008), the basis for the cycle space of $\boldsymbol{T_{PO}}$ has to be chosen according to the following criterion:

(a) the basis is given by the cycles associated with all the faces of $\boldsymbol{T_{PO}}$ except one;
(b) two cycles pass through a common edge in opposite directions.

Given a basis, the *incidence matrix* $\mathbf{C_0}$* is built, which is related to the dual graph of $\boldsymbol{T_{PO}}$ – i.e. $\boldsymbol{T_{PO}}$*, the underlying graph of the force diagram $\boldsymbol{F}$*. From the incidence matrix $\mathbf{C_0}$* of $\boldsymbol{T_{PO}}$* and the force magnitudes derived from **A**, the force diagram $\boldsymbol{F}$* is constructed, which is equivalent to the one built following the geometric procedure described in Section 2.3.1.

2.4. Construction of vector-based 3D diagrams with underlying non-planar graphs

When the underlying graph $\boldsymbol{T}$ of a given form diagram $\boldsymbol{F}$ is non-planar, different configurations of force diagrams $\boldsymbol{F}$* are available, each characterised by a specific organisation of the cycles of force vectors within the diagram. In the next subsections, a

general procedure for the construction of ***F**** is first presented that allows building ***F**** for every topology of ***F*** as long as it is in static equilibrium. Specific procedures are then described that lead to the creation of particular configurations of ***F****. As shown in Section 3, the choice of the configuration depends on the specific design problem to be solved.

2.4.1. General approach

The general strategy for the construction of ***F**** is to convert the underlying non-planar graph ***T*** of ***F*** into a *suitable* plane graph $\boldsymbol{T_P}$ and then use the latter as a reference for the generation of ***F****. A suitable $\boldsymbol{T_P}$ is one that leads to an ***F**** that still embeds the static equilibrium in ***F***, i.e. to an ***F**** where each force edge relates to a unique form edge in ***F***, is parallel to it and has a length equal to the force magnitude in it. Following the planarization, there will be more force edges in ***F**** than form edges in ***F***, which causes multiple force edges (i.e. *duplicate force edges*) to relate to the same form edge. Note that this approach can be related to other graphic statics methodologies that have also employed the addition of extra elements in response to special cases of topologies. For example, the polyhedron-based approach deals with the issue of non-planarity, albeit non-planarity in a different dimension, by using techniques such as the *zero bars* (McRobie, 2017).

In case of externally loaded structures, a preliminary operation is required before the planarization of ***T***. This consists in connecting the vertices of ***T*** that correspond to the nodes of ***F*** loaded with external forces to a single new auxiliary vertex v_E using edges e_{Ei} (Section 2.3.2). A particular drawing of ***T*** in the plane is then defined such that no e_{Ei} crosses any other edge of ***T***. Given this set up, a suitable plane graph $\boldsymbol{T_P}$ of ***T*** is obtained by successively splitting its crossing edges and reconnecting them to one or more newly introduced *auxiliary vertices* v_{Di} (Figure 6), as long as the static equilibrium of every node of the structure is fulfilled. Note that a vertex v_{Di} can be also replaced by a sub-graph representing a sub-structure of ***F*** in equilibrium with the internal forces in the edges of ***F*** corresponding to the edges of $\boldsymbol{T_P}$ connected to v_{Di}. In the simplest case, the two edges (e_s and e_t) generated after splitting an existing one ($e_{s\text{-}t}$) are reconnected to the same vertex. This transformation is equivalent to adding a new vertex $v_{s\text{-}t}$ along each crossing edge ($e_{s\text{-}t}$) – thus obtaining two new edges (e_s and e_t) for each $e_{s\text{-}t}$ – and then merging the new vertices $v_{s\text{-}t}$ into one or more new auxiliary vertices v_{Di}. In both cases, splitting must be applied until the obtained graph is planar. The number of auxiliary vertices v_{Di} has a direct impact on the number of additional cycles of force vectors in the force diagram. That number can be chosen at will by the

designer depending on the specific task at hand and the nature of the form diagram. In the next sub-sections, different ways of applying this general procedure are described.

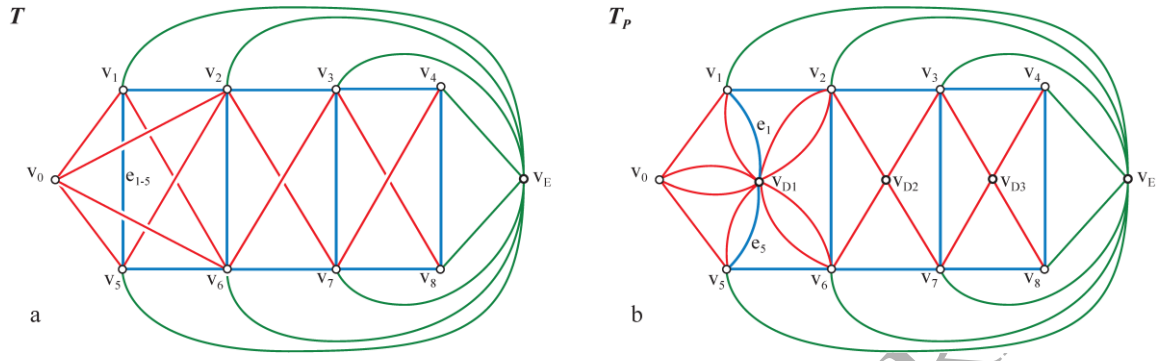

Figure 6: Example of the application of the general procedure to convert a non-planar topological graph into a plane graph; (a) non-planar graph ***T***; (b) plane graph $\boldsymbol{T_P}$ after a series of transformations.

2.4.2. Creation of a single auxiliary cycle of force vectors

As a special case of the general approach described above, in the following procedure, a new single auxiliary cycle of force vectors is generated in ***F**** after the planarization (Figure 7), other than the *cycle of external force vectors* when present. That is, each crossing edge $e_{s\text{-}t}$ of ***T*** is split into two new edges e_s and e_t that are respectively connected to the vertices v_s and v_t of $e_{s\text{-}t}$ and to one newly created auxiliary vertex v_D (Figure 7b). Like v_E, v_D does not have any corresponding node in the actual structure. The edge $E_{s\text{-}t}$ of ***F***, connected to the nodes V_s and V_t and corresponding to $e_{s\text{-}t}$ of ***T***, is substituted by a pair of opposite force vectors $\mathbf{f_s}$ and $\mathbf{f_t}$, representing respectively its internal forces $\mathbf{f_{s\text{-}t}}$ and $\mathbf{f_{t\text{-}s}}$. Hence, the vertex v_D can be regarded as the topological representation of a new sub-structure that is in static equilibrium with the internal forces in the edges of ***F*** corresponding to the split edges of ***T***. As a result, a new *auxiliary cycle of force vectors* $<V_D>^*$ is created out of the pairs of opposite force vectors corresponding to the edges of $\boldsymbol{T_P}$ connected to v_D. When this auxiliary cycle of force vectors is assembled into ***F****, two or more pairs of duplicate edges are generated in ***F**** (Figure 7d). When external forces are present, as in Figure 7, the resulting ***F**** has a *configuration with two auxiliary cycles of force vectors* $<V_E>^*$ and $<V_D>^*$ (Jasienski *et al.*, 2016). Note that different force diagrams can be assembled depending on the chosen embedding of ***T*** in the plane.

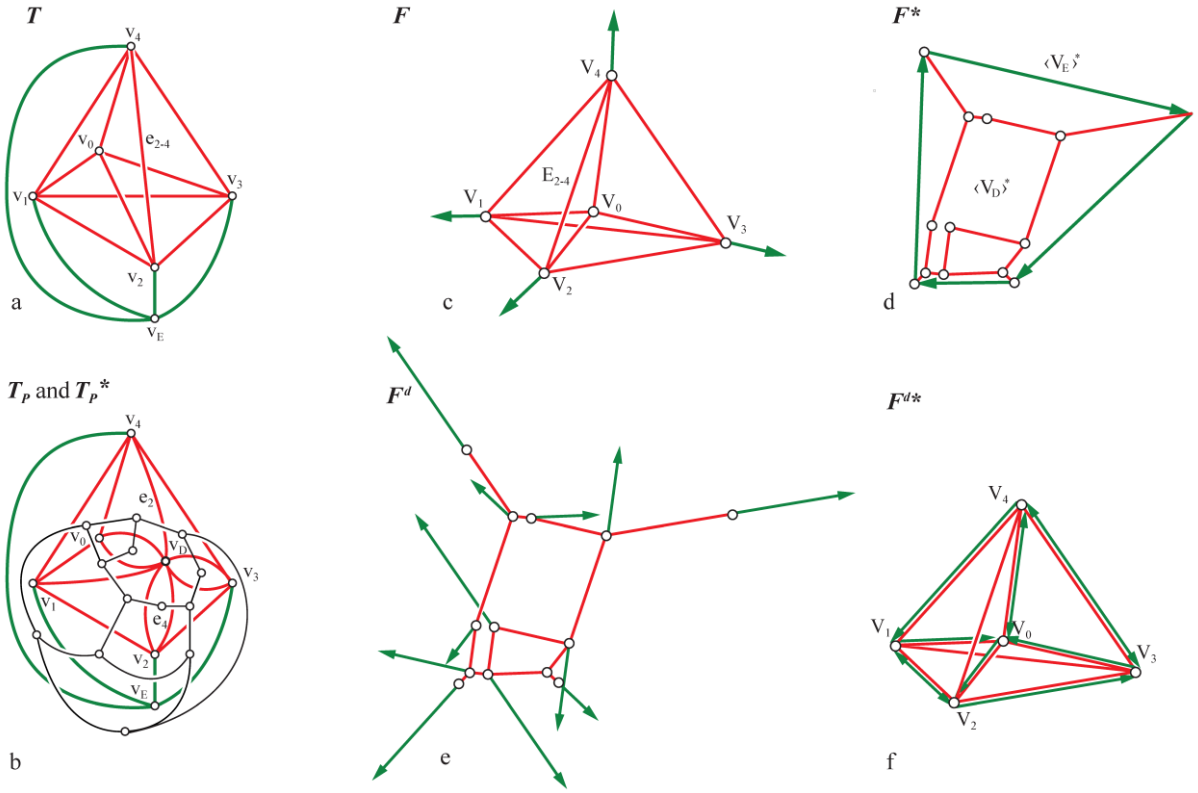

Figure 7: (a) Graph $\boldsymbol{T}$ of an externally loaded self-stressed tetrahedron; (b) plane graph $\boldsymbol{T_P}$ with one additional vertex v_D and its dual $\boldsymbol{T_P}$*; (c) vector-based 3D form diagram $\boldsymbol{F}$; (d) force diagram $\boldsymbol{F}$* with two auxiliary cycles of force vectors $\langle V_E \rangle$* and $\langle V_D \rangle$*; (e) $\boldsymbol{F}$* regarded as a structure in its own right $\boldsymbol{F^d}$; (f) force diagram $\boldsymbol{F^d}$* of $\boldsymbol{F^d}$ assembled as $\boldsymbol{F}$.

In the case of self-stressed structures (Figure 8), the force diagram has a *configuration with one auxiliary cycle of force vectors* $\langle V_D \rangle$* (Figure 8d).

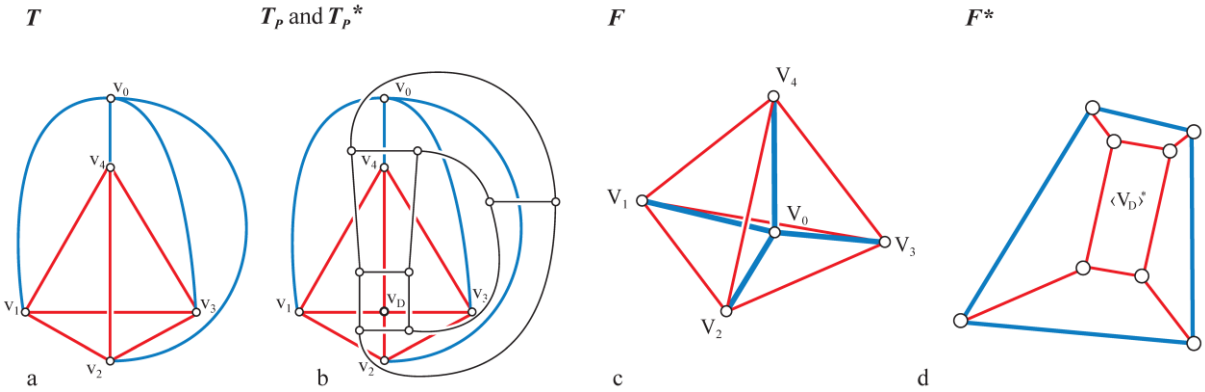

Figure 8: (a) Graph $\boldsymbol{T}$ of a self-stressed tetrahedron; (b) plane graph $\boldsymbol{T_P}$ with one auxiliary vertex v_D and its dual $\boldsymbol{T_P}$*; (c) form diagram $\boldsymbol{F}$; (d) force diagram $\boldsymbol{F}$* with one auxiliary cycle of force vectors $\langle V_D \rangle$*.

As an alternative to the previously described procedure, when external forces are present the two new edges e_s and e_t obtained after splitting each crossing edge $e_{s\text{-}t}$, can be connected to v_E rather than to v_D (Figure 9b). In this case, a closed cycle of force vectors $\langle V_E \rangle^*$ is thus generated in ***F**** in which for each pair of internal forces ($\mathbf{f_s}$ and $\mathbf{f_t}$), a pair of opposite force vectors ($\mathbf{f_s}^*$ and $\mathbf{f_t}^*$) is found in addition to the initial external forces. In comparison with the configuration with two auxiliary cycles of force vectors, this *configuration with one auxiliary cycle of force vectors* $\langle V_E \rangle^*$ generally allows minimising the number of duplicate edges (D'Acunto *et al.*, 2017).

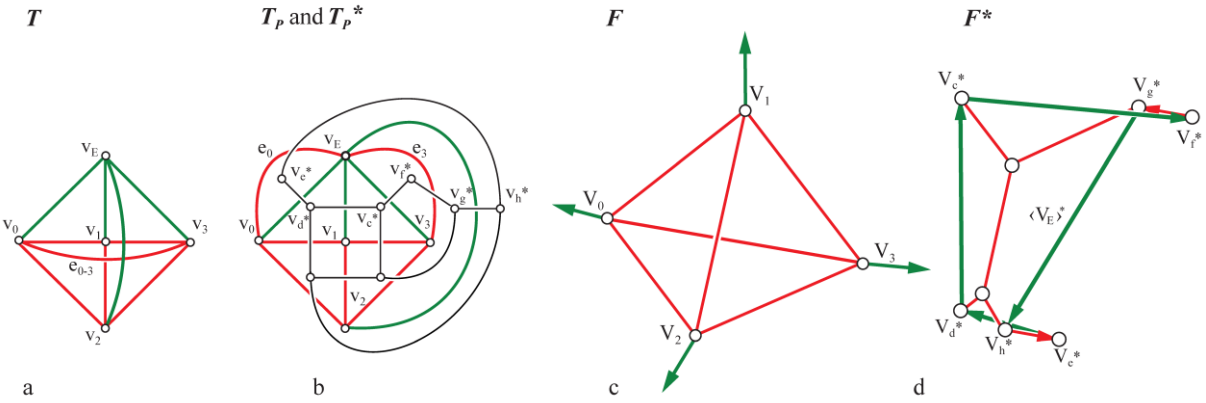

Figure 9: (a) Graph ***T*** of an externally loaded tetrahedron; (b) Plane graph $\boldsymbol{T_P}$ with two split edges and its dual $\boldsymbol{T_P}^*$; (c) vector-based 3D form diagram ***F***; (d) force diagram ***F****.

It should be noted that the resulting force diagrams ***F**** that are created following the proposed procedure are generally not reciprocal to the form diagrams ***F***, due to the presence of duplicate edges. Nevertheless, ***F*** and ***F**** are still interdependent, thus allowing their bi-directional transformation (D'Acunto *et al.*, 2017). Each node V_i of ***F*** (Figure 7c) has a corresponding closed cycle of force vectors $\langle V_i \rangle^*$ in ***F**** (Figure 7d). Moreover, if ***F**** is regarded as a structure $\boldsymbol{F^d}$ in its own right (Figure 7e), it is possible to define closed cycles of force vectors $\langle V_i^{\,d} \rangle^*$ for the nodes of $\boldsymbol{F^d}$ that can be assembled into a single force diagram $\boldsymbol{F^d}^*$ (Figure 7f), which is equivalent to ***F*** without its external forces. To generate $\boldsymbol{F^d}$ from ***F**** the force vectors of ***F**** corresponding to the external forces of ***F*** are first removed. New external forces are then introduced in $\boldsymbol{F^d}$ to achieve the equilibrium at each node V_i^d of $\boldsymbol{F^d}$ (Mitchell *et al.*, 2016), as shown in Figure 7e. These external forces are chosen so that the closed cycles of force vectors $\langle V_i^d \rangle^*$ of $\boldsymbol{F^d}^*$ (Figure 7f) are equivalent to the closed cycles of form vectors $\langle V_i \rangle$ of ***F*** (Figure 7c). It should be noted that due to the topological

transformation of $\boldsymbol{F^*}$ into $\boldsymbol{F^d}$, the construction of $\boldsymbol{F^{d*}}$ from $\boldsymbol{F^d}$ does not rely on the same graphs $\boldsymbol{T_P}$ and $\boldsymbol{T_P^*}$ used to assemble $\boldsymbol{F^*}$ from $\boldsymbol{F}$.

2.4.3. Creation of auxiliary cycles of force vectors as quads

This procedure transforms an embedding of $\boldsymbol{T}$ into a plane graph $\boldsymbol{T_P}$ by adding a new auxiliary vertex v_{Di} at every edge crossing (Buchheim *et al.*, 2013). This operation is a direct extension to 3D of the procedure introduced by Bow (1873) for the graphical solution of 2D trusses (Section 2.1). Contrary to the 2D case, however, the new auxiliary vertices v_{Di} are not related to any specific node in $\boldsymbol{F}$ since the edges of $\boldsymbol{F}$ corresponding to the crossing ones in $\boldsymbol{T}$ generally do not intersect in one point in space.

For every new auxiliary vertex v_{Di}, a new quadrilateral cycle $\langle V_{Di}\rangle^*$ constituted by two pairs of opposite force vectors is generated (Figure 10). The generated force diagram $\boldsymbol{F^*}$ has, therefore, a *configuration with multiple auxiliary cycles of force vectors as quads*. This configuration usually leads to a higher amount of duplicate edges than the other ones. Specific algorithms can be used to minimise the number of crossing edges in $\boldsymbol{T}$ during the embedding process (Chimani, 2008), in order to keep the diagram compact.

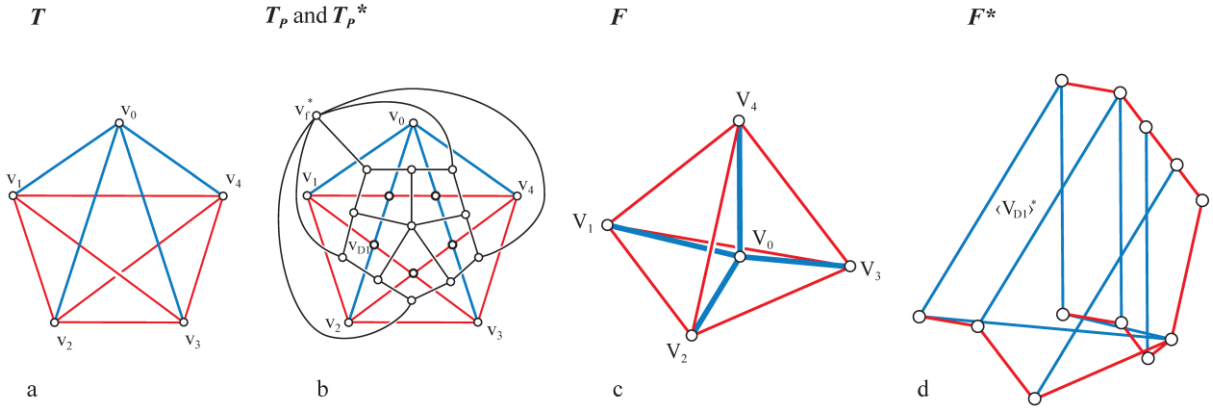

Figure 10: (a) Graph $\boldsymbol{T}$ of a self-stressed tetrahedron; (b) plane graph $\boldsymbol{T_P}$ with additional five extra vertices and its dual $\boldsymbol{T_P^*}$; (c) vector-based 3D form diagram $\boldsymbol{F}$; (d) force diagram $\boldsymbol{F^*}$ with five quadrilateral cycles $\langle V_{Di}\rangle^*$ corresponding to the auxiliary vertices v_{Di} of $\boldsymbol{T_P}$.

2.4.4. Duplication of all initial cycles of force vectors

As an extension of the planar case (Section 2.3.3), Micheletti (2008) described a procedure to find the reciprocals $\boldsymbol{F^*}$ of some 3D self-stressed networks with underlying non-planar graphs. Based on a modification of the criterion stated in Section 2.3.3, the choice of a basis for the cycle space in $\boldsymbol{T}$ needs to meet the following requirements:

(a) each edge belongs precisely to two cycles in the basis;

(b) two cycles share at most two edges;

(c) when two cycles share two edges, the cycles travel one edge in opposite directions and the other edge in the same direction.

When such requirements are met, the incidence matrix **C*** of ***F**** is generated and used to assemble the force diagram. The latter has a *point-symmetric configuration*, i.e. the nodes and edges of ***F**** are repeated twice within the diagram and are arranged symmetrically about the same symmetry point (Figure 11d). Because all the elements of ***F**** are duplicated, the number of edges in ***F**** is exactly double than the one in the given ***F***.

The same *point-symmetric* ***F**** can be obtained from the given ***F*** in compliance with the topological approach introduced in this paper. As described in Section 2.4.2, the crossing edges in ***T*** (Figure 10a) are first split and connected to a new vertex v_D to generate the plane graph $\boldsymbol{T_P}$ (Figure 11a). Without altering the equilibrium of the structure, the graph $\boldsymbol{T_P'}$ can be constructed by replacing the vertex v_D of $\boldsymbol{T_P}$ with a sub-graph corresponding to a sub-structure that is in static equilibrium with the internal forces in the edges of ***F*** corresponding to the split edges of ***T***. A possible sub-structure is the one constituted by the edges of ***F*** that do not correspond to crossing edges in the initial ***T***. In this case, the new graph $\boldsymbol{T_P'}$ is generated (Figure 11b) in which all the edges of the initial ***T*** (Figure 10a) are repeated twice. In the corresponding form diagram $\boldsymbol{F_P'}$ (Figure 11c) all the edges and nodes of the initial ***F*** (Figure 10c) are repeated twice and overlapped on each other. The reciprocal force diagram ***F**** (Figure 11d) has a *point-symmetric configuration*, while $\boldsymbol{T_P'}$ and $\boldsymbol{T_P^{*'}}$ are dual graphs (Figure 11b).

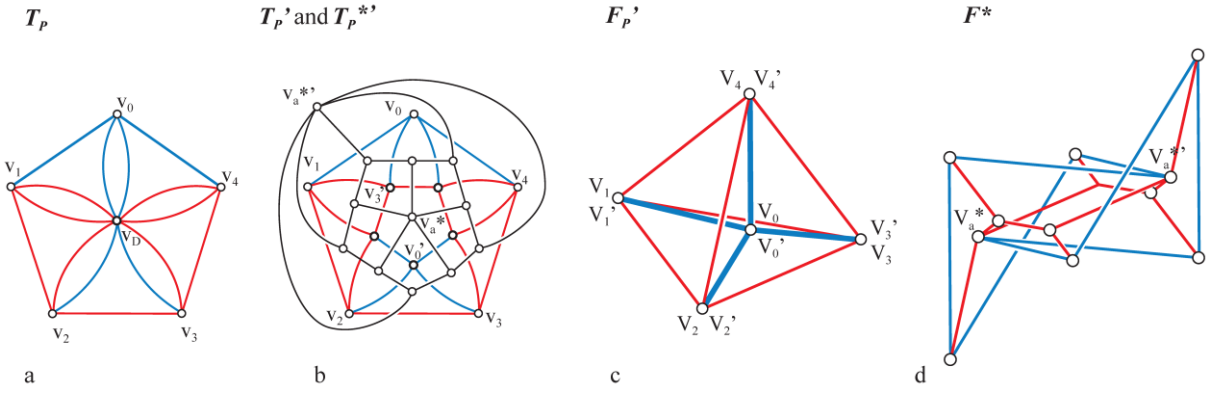

Figure 11: (a) Plane graph $\boldsymbol{T_P}$ of a self-stressed tetrahedron (Figure 10c); (b) plane graph $\boldsymbol{T_P'}$ in which all the edges of the initial ***T*** (Figure 10a) are repeated twice, and its dual $\boldsymbol{T_P^{*'}}$; (c) vector-based 3D form diagram $\boldsymbol{F_P'}$

with duplicated nodes and edges in relation to the initial ***F*** (Figure 10c); (d) point-symmetric reciprocal 3D force diagram ***F****.

In this way, the procedure introduced by Micheletti can be directly related to the one described in Section 2.4.2 for self-stressed structures. That is, a given ***F**** with *one auxiliary cycle of force vectors* (Figure 8d) can be converted into ***F****$^{'''}$ with a *point-symmetric configuration* if the force vectors within the individual cycles $<V_i>^*$ and $<V_D>^*$ of ***F**** can be arranged, so that duplicate edges lie topologically opposite to each other. To obtain the ***F****$^{'''}$ (Figure 12c), at first the ***F**** is deprived of $<V_D>^*$ to generate ***F****$^{'}$ (Figure 12a); this is then duplicated and mirrored into ***F****$^{''}$ (Figure 12b). The ***F****$^{'}$ and ***F****$^{''}$ are eventually assembled into ***F****$^{'''}$ (Figure 12c).

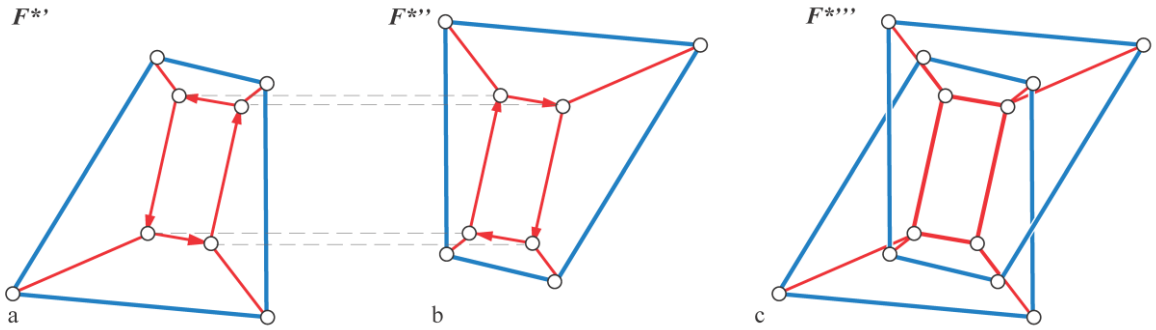

Figure 12: (c) Point-symmetric force diagram ***F****$^{'''}$ – from the assembly of (a) ***F****$^{'}$ and (b) ***F***$^{''}$ – relative to the form diagram ***F*** of Figure 8c.

3. Application of vector-based 3D graphic statics to structural design

The approach for the construction of 3D force diagrams for given 3D form diagrams described in the previous section, together with the possibility of transforming these diagrams (D'Acunto *et al.*, 2017) and using related form-finding techniques like the Combinatorial Equilibrium Modelling (CEM) (Ohlbrock *et al.*, 2016), constitute the basis of the proposed design framework grounded on vector-based 3D graphic statics. In this section, two conceptual design case studies are presented to demonstrate the potential application of the proposed framework to realistic design scenarios.

The conceptual stage of the design process is the phase during which the main concept of a structural project is defined. This moment is of crucial importance as it frames the scope for all further subsequent design refinements. Authors have shown the importance to operate with interactive and concise tools at this stage (Krasny, 2008; Fivet and Meng, 2017). In this context, the proposed design framework based on vector-based 3D form and force diagrams is

unique. While being visually intelligible, the diagrams are easily exploited to explore in real-time the direct relationship between the form of a structure and its inner forces, thus representing an operative medium for structural design (Kotnik and D'Acunto, 2013). As such, the use of the diagrams would not only provide the experienced designers with a complete and direct tool to explore and compare different design solutions but also facilitate the less experienced designers to approach the structural design problem more responsively and intuitively.

3.1. First case study: a pedestrian suspension bridge

The structural concept for a pedestrian suspension bridge is laid out according to a fictitious design scenario. Specifically, the deck of the bridge has to be hung below one main suspension cable on twenty-four secondary hangers. The deck has to be anchored on two given support points, which are 80.0 m apart from each other. The main cable should be suspended between two pylons. Given this setup, the task is to suggest a proposal for the overall geometry of the bridge considering a predefined uniformly distributed load on the deck of 10 kN/m.

The first instance of the geometry is generated using CEM (Ohlbrock *et al.*, 2016). Specifically, the main suspension cable of the bridge is modelled as two opposite trails that originate at the centre of the bridge, each made of twelve *trail members*; the same approach is adopted for the deck with eleven *trail members* (Figure 13). The hangers are then regarded as *direct deviation members*. The elements representing the suspension cable and the hangers are set to tension, while the ones related to the deck and the pylons to compression. A preliminary form diagram (Figure 14a, left, in grey) and force diagram (Figure 14a, right, in grey) are then created by fixing the four *start nodes* of the form diagram on a vertical plane π. Since the underlying graph $\boldsymbol{T}$ of the structure is planar, the procedure described in Section 2.3.2 is used to assemble the force diagram. The two start nodes related to the suspension cable are subsequently moved out of the vertical plane π. The magnitude of the applied external loads is then calculated according to the resulting tributary length of the deck. This operation results in the generation of the form $\boldsymbol{F}$ (Figure 14a, left, in colours) and the force $\boldsymbol{F^*}$ (Figure 14a, right, in colours) diagrams**.**

In the second design step a parallel shear transformation and a non-uniform scaling along the **y**-axis are applied. These global transformations are used to adjust $\boldsymbol{F}$ (Figure 14b, left, in grey) into $\boldsymbol{F'}$ (Figure 14b, left, in colours) to meet the given fictitious support constraints. The

same transformations are applied to ***F**** (Figure 14b, right, in grey) that is converted into ***F*'*** (Figure 14b, right, in colours). Because of their underlying properties (Pottman *et al.*, 2007), global parallel transformations do not break the interdependence between the diagrams, i.e. corresponding edges in the diagrams stay parallel after the transformation (Huerta, 2010).

In the third design step, due to the variation of the lengths of the deck members, a series of local transformations are performed. The recourse to local transformations makes it possible to operate only on specific elements of the force diagram and assess the consequent transformation of the form diagram. Here, local adjustments are used to update the magnitudes of external forces in ***F*'*** (Figure 14c, right, in grey) and to find an equilibrium state ***F''*** (Figure 14c, left, in colours) for which all hangers, respectively all suspension cable elements, have the same force magnitudes, as shown in ***F*''*** (Figure 14c, right, in colours).

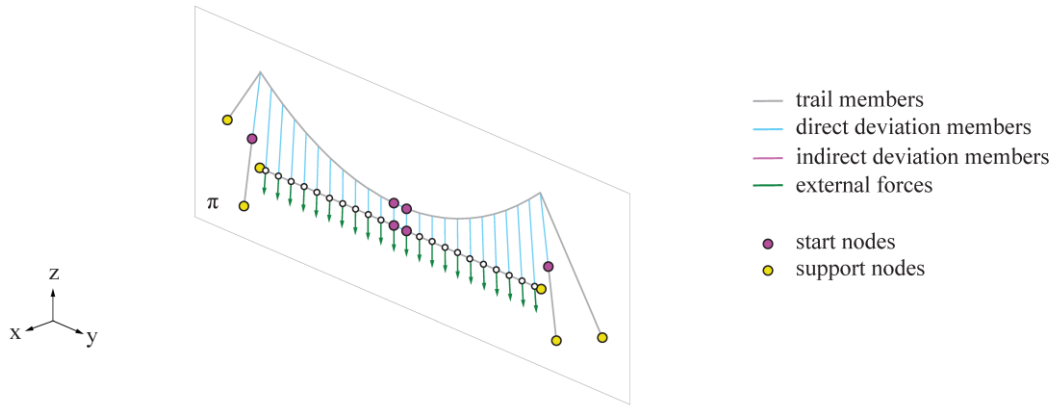

Figure 13: Conceptual design of a pedestrian bridge: initial set-up for the form-finding

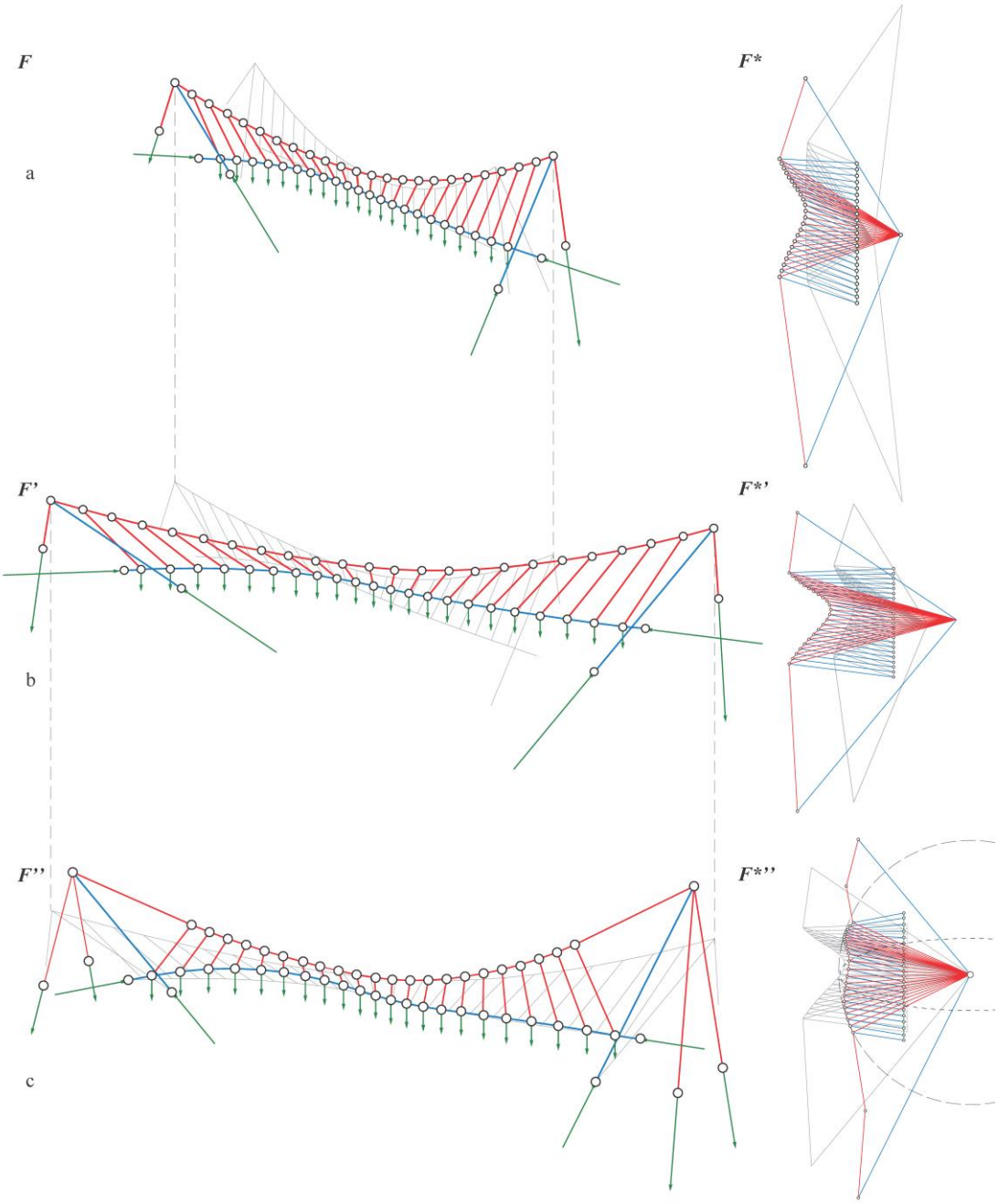

Figure 14: Conceptual design of a pedestrian bridge: (a) initial equilibrium state; (b) equilibrium state after global transformations; (c) equilibrium state after local transformations

To secure the interdependence between ***F''*** and ***F*"*** during the transformation, corresponding edges in the two diagrams are constrained to stay parallel. The resulting constrained non-linear problem is here solved using customised *Python* scripts within the CAD platform *McNeel Rhinoceros* and the *Kangaroo2* library by Piker (2017), whose solver is built around a specific implementation of position-based dynamics (Bender *et al.*, 2015). As can be seen from ***F*''*** (Figure 14c, right, in colours), constraining a constant force in the suspension cable

elements, is equivalent to constrain all corresponding force vectors to lie on the surface of a sphere, whose radius is equal to the target force magnitude.

As a last design step, to stabilise the pylons against lateral loadings, the tension cable connecting them to the ground is replaced by two cables. The resulting conceptual design state of the bridge (Figure 15) can then be used as a starting point for further design developments, such as stiffening the structure against secondary loadings.

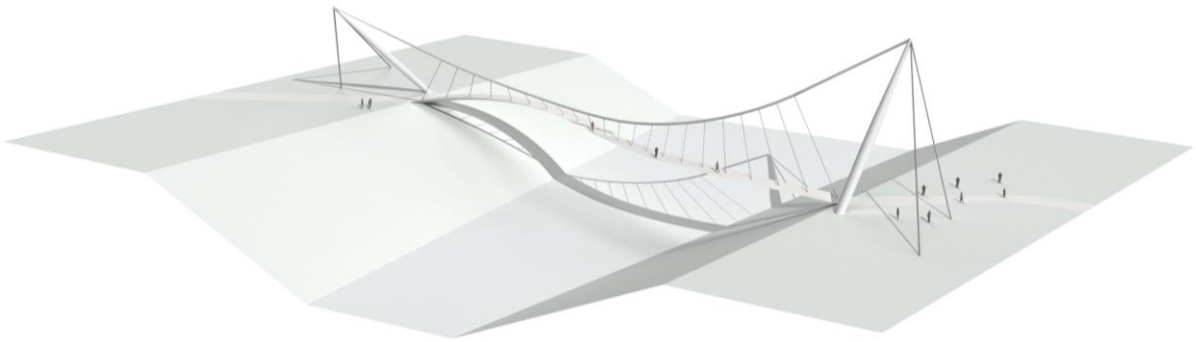

Figure 15: Conceptual view of the pedestrian suspension bridge designed using the proposed vector-based 3D graphic statics framework

3.2. Second case study: a spoked wheel roof for a stadium

A fictitious setting is defined to guide the design of a stadium roof in the shape of a spoked wheel. The roof has to be built around a standard football pitch of 90m by 120m. The roof should be constituted by one inner tension ring and two outer compression rings, the former and the latter being connected by spokes in tension. Moreover, a simplified dominant load case is introduced that combines a pre-stressing force in the inner tension ring (10 000 kN) and a vertical load of 5 kN/m^2 applied as punctual loads (250 kN each) on the nodes of the tension ring and the lower outer compression ring. These loads reflect the presence of roof panels supported on these two rings.

As in the previous case study, in the first step, a preliminary geometry of the roof is generated using CEM. In this case, forty trails are introduced in $\boldsymbol{T}$ to model the spokes of the wheel, each one connecting a start vertex, where an external load is applied, to a support vertex. Moreover, three closed sequences of direct deviation members are defined, which represent the rings of the roof, i.e. the inner one in tension and the outer ones in compression.

Additionally, *indirect deviation members* are introduced that connect the inner ring to the outer lower ring (Figure 16). In this first design iteration, the start nodes are placed equally distanced on a circle *c* with a radius of 60.0 m, which defines the geometry of the inner ring. The length of the spokes is also set to 60.0 m.

Contrary to the previous case study, here the underlying graph ***T*** of the structure is non-planar. Hence, one of the alternative procedure described in Section 2.4 has to be used to assemble the force diagram ***F****. In the first design step, the procedure described in Section 2.4.2 is initially chosen (Figure 17a, right) to keep the diagram compact and minimise the number of non-overlapping pairs of vectors.

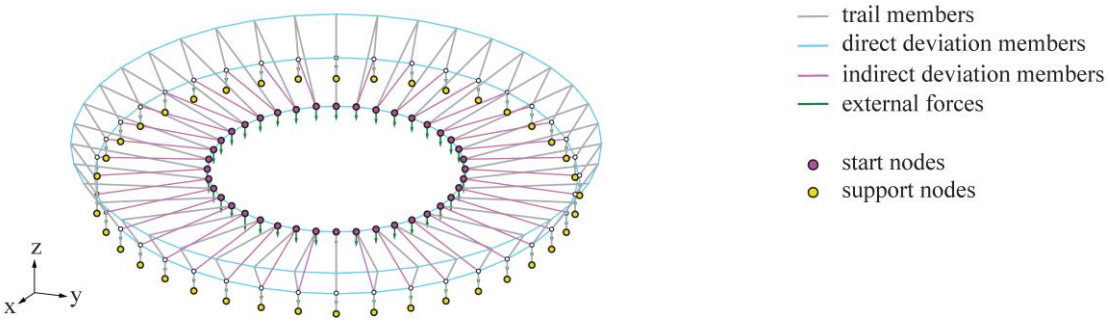

Figure 16: Conceptual design of a spoked wheel stadium roof: initial setup for the form finding

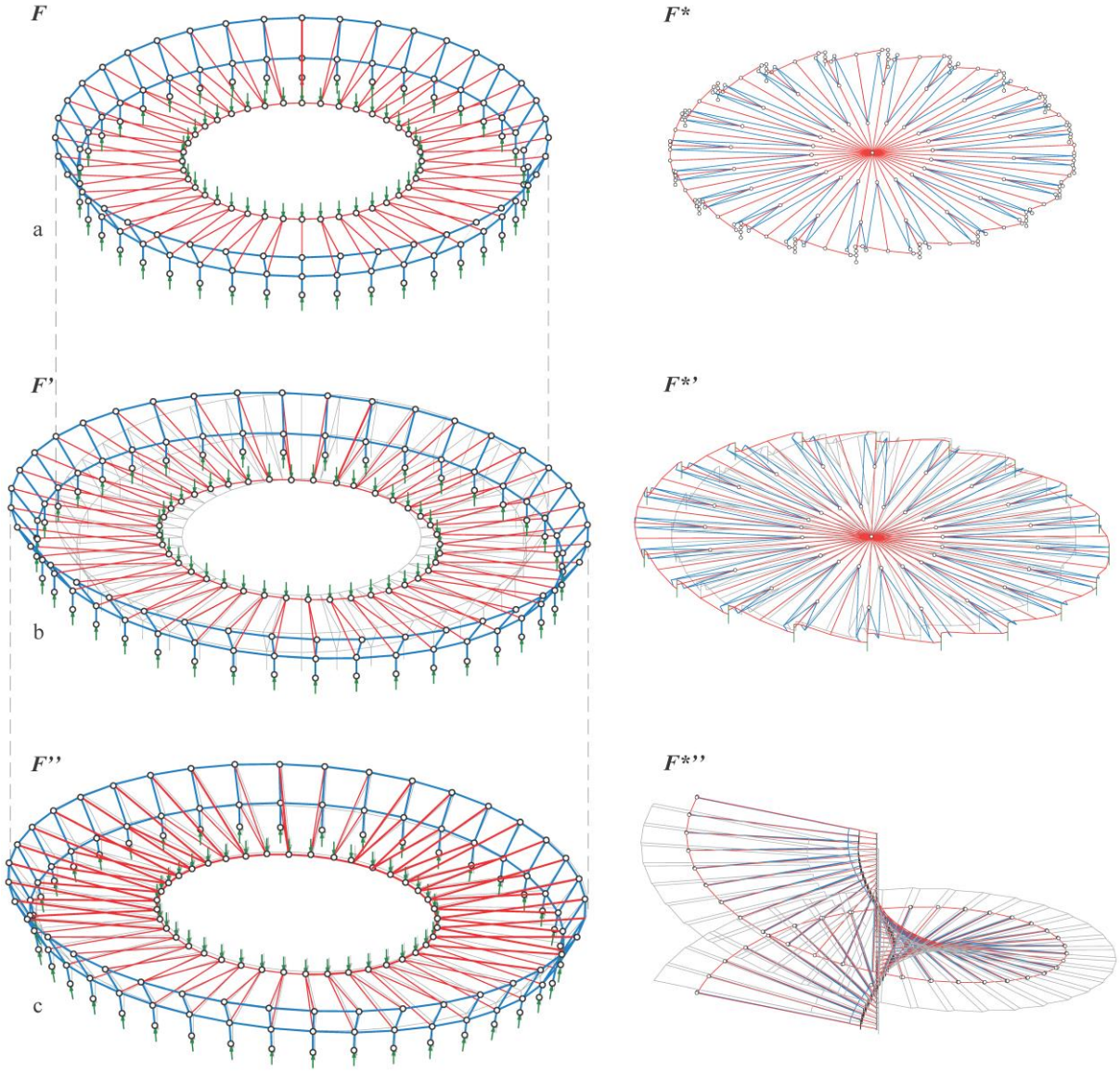

Figure 17: Conceptual design of a spoked wheel stadium roof: (a) initial equilibrium state based on form ***F*** and force ***F**** diagrams; (b) equilibrium state after global transformations of ***F*** and ***F**** (in grey) into ***F'*** and ***F*'*** (in colours); (c) equilibrium state after local transformations, leading to the final form ***F''*** and force ***F*''*** diagrams (in colours); note that in this case a topologically different force diagram configuration is adopted in comparison to the one used in the previous steps.

In the second design step, a global non-uniform scaling along the **y**-axis is applied to ***F*** (Figure 17b, left, in grey) and ***F**** (Figure 17b, right, in grey) to adjust the initial geometry of the roof to the layout of a football pitch, thus generating ***F'*** (Figure 17b, left, in colours) and ***F*'*** (Figure 17b, right, in colours). In the third design step, a customized force diagram configuration (Figure 17c, right, in grey), which is topologically different from the one used in the previous steps, is adopted. This force diagram configuration is based on the general strategy defined in Section 2.4.1 and, in comparison to the previous one, it allows having

better control of the individual external force vectors. The magnitudes of the inner forces as well as of the applied external forces are individually adjusted through local transformations, to produce ***F*"*** (Figure 17c, right, in colours). As in the previous case study, local transformations are executed in a nonlinear fashion, while constraining the position of the nodes of the inner tension ring and the supports in ***F''*** (Figure 17c, left, in colours). As a result of the increment of magnitudes of applied external forces along the longitudinal side of the roof, the upper outer ring, which was initially contained in a plane (Figure 17c, left, in grey), gains a three-dimensional shape with variable static height (Figure 17c, left, in colours). A conceptual view of the stadium is shown in Figure 18. It can be regarded as a base for subsequent design refinements.

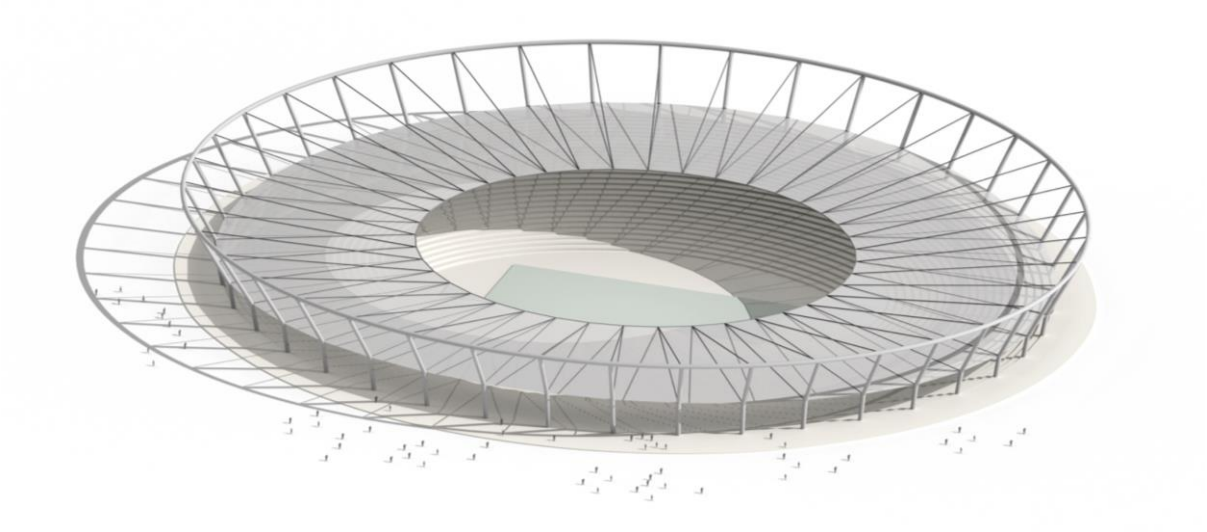

Figure 18: Conceptual view of the stadium roof designed using the proposed vector-based 3D graphic statics framework

4. Discussion and Conclusion

This article introduced a complete framework based on the vector-based approach to 3D graphic statics. The framework supports the design of any class of spatial networks in static equilibrium while allowing the designer to control in real time the force magnitudes and the geometry of the structure.

After defining a series of geometric constructions to assess the magnitude of forces within a given spatial network in equilibrium, various procedures for the construction of vector-based 3D force diagrams were presented. The resulting form and force diagrams are generally not reciprocal because they have different numbers of edges, nodes and cycles. However, the diagrams maintain parallelism between all corresponding edges and are direct interpretations

of dual graphs. It is therefore convenient to handle both diagrams simultaneously through bi-directional transformations. By taking advantage of digital tools for computer-aided design, the proposed framework can be directly implemented into a series of parametric definitions, which allow for the real-time and interactive manipulation of both form and force diagrams throughout the structural design process. The resulting immediacy of control of the diagrams by the user is beneficial for design. For instance, the geometry of a given structural network can be adjusted in order to reduce the magnitudes of its inner forces, or the structural form can be found by imposing a specific distribution of inner forces.

As shown in two case studies, vector-based 3D form and force diagrams are appropriate to be used as active design tools to generate and refine complex spatial structures. Thanks to the manipulation of the forces within a spatial network, a quick exploration of valid static equilibrium solutions can be performed during the design process. At the same time, a visual and intuitive understanding of the structural behaviour of the modelled structures is provided. In this regard, the authors foresee that this approach will support the emergence of new structural typologies while fostering creativity in the structural design process.

References

Akbarzadeh M., Van Mele T. and Block P., 2015: On the Equilibrium of Funicular Polyhedral Frames and Convex Polyhedral Force Diagrams, *Computer-Aided Design*, **63**; 118-128.

Alic V. and Akesson D., 2017: Bi-directional algebraic graphic statics, *Computer-Aided Design*, **93**; 26-37.

Bender J., Müller M. and Macklin M., 2015: Position-Based Simulation Methods in Computer Graphics, in Zwicker M. and Soler C. (eds.) *Eurographics 2015 – Tutorials*.

Bow R., 1873: Economics of Construction in Relation to Framed Structures, London: E. and F.N. Spon.

Buchheim C., Chimani M., Gutwenger C., Jünger M. and Mutzel P., 2013: Crossings and planarization, in Tamassia R., *Handbook of Graph Drawing and Visualization, Discrete Mathematics and its Applications*, Boca Raton: CRC Press.

Calladine C. R., 1978: Buckminster Fuller's 'Tensegrity' Structures and Clerk Maxwell's Rules for the Construction of Stiff Frames, *International Journal of Solids and Structures*, **14**: 161–172.

Chimani M., 2008: Computing Crossing Numbers, PhD dissertation, Technical University of Dortmund.

Crapo H., 1979: Structural Rigidity. *Structural Topology*, **1**; 19.

Crapo, H. and Whiteley, W., 1993: Plane self stresses and projected polyhedra I: the basic pattern, *Structural Topology*, **20**, 55–78.

Cremona L., 1872: Le figure reciproche nella statica grafica, Milano: Tipografia Bernardoni.

Culmann C., 1866: Die Graphische Statik, Zurich: Von Meyer & Zeller.

D'Acunto P., Jasienski J. P., Ohlbrock P. O. and Fivet C., 2017: Vector-Based 3D Graphic Statics: Transformations of Force Diagrams, *Proceedings of the IASS 2017,* Hamburg.

D'Acunto P., Ohlbrock P. O., Jasienski J. P. and Fivet C., 2016: Vector-Based 3D Graphic Statics (Part I): Evaluation of Global Equilibrium, *Proceedings of the IASS 2016,* Tokyo.

Fivet C., 2016: Projective transformations of structural equilibrium, *International Journal of Space Structures*, **31**(2-4), 135 –146.

Fivet C. and Meng X., 2017: Digital Graphic Statics – Shared Design Tools for Architects and Engineers. *Architectural Journal, China*, **590**: 20-25.

Fivet C. and Zastavni D., 2012: Key methods from Robert Maillart's Salginatobel design process. *J Int Assoc Shell Spat Struct*, **53**: 39–47.

Harary F., 1969: Graph theory, Reading, Massachusetts: Addison-Wesley.

Huerta S., 2010: Designing by geometry: Rankine's theorems of transformation of structures, in Cassinello P. (ed.), *Geometry and proportion in structural design, essays in Ricardo Aroca's Honour*, Madrid, 263–285.

Jasienski J. P., D'Acunto P., Ohlbrock P. O. and Fivet C., 2016: Vector-Based 3D Graphic Statics (Part II): Construction of Force Diagrams, *Proceedings of the IASS 2016,* Tokyo.

Jasienski J. P., Fivet C. and Zastavni D., 2014: Various perspectives on the extension of graphic statics to the third dimension, *Proceedings of IASS-SLTE 2014*, Brasilia.

Jessen B., 1967: Orthogonal icosahedron, *Nordisk Mat. Tidskr*., **15**; 90-96.

Konstantatou, M., D'Acunto, P. and McRobie, A. 2018: Polarities in Structural Analysis and Design: n-dimensional Graphic Statics and Structural Transformations, *International Journal of Solids and Structures*;**152–153**, 272-293.

Kotnik T., D′Acunto P., 2013: Operative Diagramatology: Structural Folding for Architectural Design, *Proceedings of Design Modelling Symposium*, Berlin, 193-203.

Krasny E. (ed.), 2008: The force is in the mind, the making of architecture. Architekturzentrum Wien, Birkhäuser, Basel Boston Berlin.

Lee J., Van Mele T. and Block P., 2018: Disjointed force polyhedra, *Computer-Aided Design;* **99**, 11-28.

Mackinlay J., 1986: Automating the design of graphical presentations of relational information, *Transactions on Graphics*; 5(2); 110-141.

Maxwell J.C., 1864: On reciprocal figures, frames and diagrams of forces, *Philosophical Magazine,* **27**; 250–61.

Maxwell J.C., 1867: On the application of the theory of reciprocal polar figures to the construction of diagrams of forces, *The Engineer*, **24**.

McRobie A., 2017: The geometry of structural equilibrium, *R. Soc. open sci.* **4**: 160759.

Micheletti A., 2008: On generalized reciprocal diagrams for self-stressed frameworks, *International Journal of Space Structures*, **23(3)**; 153-166.

Mitchell T., Baker W., McRobie A. and Mazurek A., 2016: Mechanisms and states of self-stress of planar trusses using graphic statics, part I, *International Journal of Space Structures*, **31** (2-4); 85 –101.

Ohlbrock P. O., D'Acunto P., Jasienski J. P. and Fivet C., 2016: Vector-Based 3D graphic statics (Part III): Designing with Combinatorial Equilibrium Modelling, *Proceedings of the IASS 2016*, Tokyo.

Pellegrino S. and Calladine C. R., 1986: Matrix Analysis of Statically and Kinematically Indeterminate Frameworks, *International Journal of Solids Structures*, **22**; 409-428.

Piker D., 2017: Kangaroo2, http://www.food4rhino.com/app/kangaroo-physics, ver. 2.42 (accessed 15/09/2018).

Pirard A., 1950: La Statique Graphique, Imprimerie H. Vaillant-Carmanne S.A.

Pottman H., Asperl A., Hofer M. and Kilian A., 2007: Architectural Geometry, Bentley Institute Press.

Rankine, W. J. M., 1864: Principle of the equilibrium of polyhedral frames, *The London, Edinburgh, and Dublin Philosophical Magazine and Journal of Science XXVII* - Fourth Series (CLXXX - February), 92.

Sauer R., 1970: Differenzengeometrie, Berlin: Springer.

Saviotti C., 1888: La Statica Grafica. Seconda Parte: Forze Esterne, Milano: Ulrico Hoepli.

Tachi T., 2012: Design of infinitesimally and finitely flexible origami based on reciprocal figures, *J Geom Graph*, **16**; 223–234.

Tamassia R. (ed.), 2013: Handbook of Graph Drawing and Visualization, CRC Press.

Van Mele T. and Block P., 2014: Algebraic Graph Statics, *Computer-Aided Design*, **53**; 104-116.

Wallner J. and Pottmann H., 2008: Infinitesimally flexible meshes and discrete minimal surfaces, *Monat Math*, **153**: 347–365.

Whitney H., 1933: Planar graphs, *Fund. Math*., **21**; 73-84.